平成２６年度　厚生労働科学研究費補助金

（新型インフルエンザ等新興・再興感染症研究事業（新興・再興感染症に対する革新的医薬品等開発推進研究事業））

結核感染肺における IL-17 依存性肉芽腫形成メカニズムの解明

分担研究報告書

研究分担者

梅村　正幸

（琉球大学・准教授）

厚生労働科学研究費補助金（新型インフルエンザ等新興・再興感染症研究事業（新興・再興感染症に対する革新的医薬品等開発推進研究事業））
分担研究報告書

結核感染肺における IL-17 依存性肉芽腫形成メカニズムの解明

研究分担者　梅村　正幸　（琉球大学熱帯生物圏研究センター・生体防御学・准教授）
研究協力者　福井　雅之　（琉球大学熱帯生物圏研究センター・ポスドク研究員）

研究要旨.
結核を制圧するためには、結核菌に対して有効な防御免疫応答を誘導するワクチンの開発が重要課題と考えられる。本研究では、結核菌感染肺での肉芽腫形成における IL-17 関連因子発現機構を解明するために、肺内肉芽腫形成を誘導するモデルを作製し、遺伝子発現様式を解析した。

A. 研究目的

結核は 20 世紀最大の恐怖を与えた慢性持続性感染症であり、依然としてその罹患率は著しく高く、国際レベルで大きな社会問題となっており、その制圧は急務とされている。現在、多くの国で結核菌ワクチン株 *Mycobacterium bovis*Bacille de Calmette et Guérin (BCG)の皮内接種が行われている。しかし、小児の結核性髄膜炎ならびに粟粒結核に対しては高い防御効果を示しているが、高齢者のみならず、若年・青年層の結核の増加が目立ち、既存の BCG の結核予防効果の低さが問題視されている。また、近年では不規則な薬剤供給や不適切な処方などにより、抗結核薬の効かない多剤耐性結核菌が熱帯・亜熱帯地域を含む世界各地で検出されており、化学療法による治療が困難である症例が増多している。こういった現状を打破するためには、より有効なワクチンの開発と発症予防法および治療法の確立が急務であり、結核制御上最重要課題であると思われる。そのためにも、動物感染モデルにおいて結核菌による病態形成あるいはその制御に関与する因子を見出し、その分子基盤を明らかにすることが必要である。

我々は炎症性サイトカインとして知られる Interleukin(IL)-17 に着目し、その細胞内寄生性細菌に対する感染防御機構について追究してきた。細胞内寄生性細菌、特に結核菌を代表とするマイコバクテリアに対する防御としての IL-17A の重要性を見出し報告している。また同時に、結核菌の病態形成の特徴の一つである肉芽腫の形成、成熟ならびにその維持に IL-17A が深く関与していることを見出している。一方、IL-17A は IL-17 サイトカイン・ファミリーに属しており、そのサイトカイン・ファミリーの中でも IL-17F は、IL-17A とアミノ酸レベルで最も相同性が高く、共通の受容体を利用することから、IL-17F は結核菌感染に対して IL-17A と同程度の防御性を有すると考えた。昨年度、結核菌慢性感染における IL-17 サイトカイン・ファミリーの防御能を各々の遺伝子欠損(KO)マウスを用いて検証したところ、IL-17A KO マウスでは著しい生存率の低下が認められたものの、IL-17F KO マウスでは正常マウスと同等レベルであり、各臓器の排菌能も IL-17F KO マウスは正常マウスと同等であった。しかし、感染早期における IL-17F の結核菌に対する感染防御能を検討した結果、感染早期では IL-17A 同様、感染防御に働くが、感染後期においてはその効果が非常に低くなる

ことが明らかになった。この現象をより詳細に理解するため、マイコバクテリア感染肺における IL-17F の関与を詳細に検討した。

上記で検討した IL-17 サイトカイン・ファミリーの一つである IL-17F は IL-33 により産生誘導されることが報告されている。IL-33 は細胞核内に蓄積される損傷関連分子パターン（damage-associated molecular pattern：DAMP）として知られており、我々の先行研究により、マイコバクテリア感染により肺で放出されることを見出している。IL−1 サイトカイン・ファミリーに属する IL-33 は、その受容体である ST2L と IL-1RAcP を介して 2 型免疫応答を誘導するサイトカインである。以前、ST2 KO マウスを用いた結核菌肺感染モデルにおいて、ST2 KO マウスは正常マウスにおける免疫応答と変わらないことが報告されている。しかしながら、マイコバクテリア感染肺における IL-33 の自然免疫制御に関しては未だ不明瞭な点が多い。本研究では IL-33 KO マウスを用い、マイコバクテリア感染早期における IL-33 の防御効果を検討した。

B. 研究方法

(1) マイコバクテリア感染肺における IL-17F 産生細胞の同定とその局在性

8-10 週齢雌の C57BL/6N マウスに 5 x 10^6cfu の *Mycobacteriumbovis*BCG を経気道感染させ、経時的に肺組織を採取した。Total RNA を精製した後、cDNA 合成し real-time RT-PCR で IL-17F 発現の動態を調べた。さらに、感染 28 日目のリンパ球を調製し、フローサイトメトリーで IL-17F 産生細胞の同定を試みた。*In vitro* 系としては、マウス II 型肺胞上皮細胞株である MLE-15、MLE-12 および LA4 細胞を用いて、BCG 感染における IL-17F の発現誘導を確認した。*In vivo* 系で IL-17F 産生細胞の同定およびその局在性は、BCG 感染肺を免疫染色法を用いて観察した。

(2)結核菌慢性感染における IL-33 の防御機構の解析

1x10^3cfu の *Mycobacterium tuberculosis* H37Rv 株を 8-10 週齢雌の野生型(C57BL/6)および IL-33 KO マウスに経気道感染させ、生存率をモニタリングした。同時に感染 120 日後の臓器内菌数を調べた。また、結核菌感染における肉芽腫形成への IL-17F の関与は、肺の病理組織学的解析を行った。さらに、*M. bovis* bacilli Calmette-Guérin (BCG)を野生型 C57BL/6 あるいは IL-33 KO マウスに経気道感染させ、臓器内菌数を比較した。In vitro 系の実験で、NF-κB の転写応答配列の下流に分泌型アルカリホスファターゼ遺伝子を組み込んだ組換え RAW264.7 細胞を用いて、BCG 感染時における IL-33 存在/非存在下での NF-▪B 活性の活性化を調べた。さらに、同条件下での誘導性 NO 合成酵素(iNOS)や各種抗菌性ペプチド（lipocalin-2、S100A8 等）の発現増強を real-time RT-PCR で検討した。

倫理面への配慮　本研究で行われる遺伝子組換え生物等使用実験は「遺伝子組換え生物等の使用等の規制による生物多様性の確保に関する法律」およびこれに関係する施行規則並びに省令に従って計画され、琉球大学遺伝子組換え生物等使用安全管理規則の定めるところによって安全委員会の認可を受けたのちに実施された。また、本研究での動物使用実験については、琉球大学動物実験委員会に研究計画の審査を受け、動物実験における生命倫理に適合することを承認された後に行なわれた。

C. 研究結果

(1) マイコバクテリア感染肺における IL-17F 産生細胞の同定とその局在性

BCG 感染肺における IL-17F の発現動態を調べた結果、感染後 IL-17F の発現増強傾向が認められた。そこで、IL-17F 産生細胞の同定を試みた結果、リンパ球からの IL-17F 産生は観察できず、IL-17F 産生細胞は非造血系細胞である可能性が考えられた。*In vitro* 系の解析において、マウス II 型肺胞上皮細胞株である MLE-15、MLE-12 ならびに LA4 は非感染の状態でも高レベルに IL-17F を発現し、かつ BCG 感染することにより有

意に高い IL-17F 発現が示された。また、IL-17F の BCG 感染肺における分布を検討したところ、肉芽腫構造の内側には IL-17F はほとんど認められず、肉芽腫の周囲に存在していた。さらに、II 型肺胞上皮細胞特異的マーカーである Surfactant protein-C と IL-17F を多重染色したところ、両者が共局在することが確認できた。

(2)結核菌慢性感染における IL-33 の防御機構の解析

結核菌慢性感染における IL-33 の関与を IL-33 KO マウスを用いて検証したところ、結核菌感染において IL-33 KO マウスは野生型マウスと同等レベルであった。また、慢性感染肺（感染 120 日）の菌の排除能も IL-33 KO マウスは野生型マウスと差が認められなかった。付け加えるのならば、肉芽腫形成にも炎症性サイトカイン（IFN-γ、TNF-αおよび IL-6）の発現にも顕著な差が認められなかった。これらのことから、結核菌の慢性感染肺では IL-33 は積極的に感染防御に関与していないと考えられた。その仮説をより詳細に検証するため、感染早期における IL-33 の結核菌に対する感染防御能を検討した。感染早期の解析はその影響(動態)が簡便な BCG を用いて検討した。BCG 感染における感染 28 日後の肺内菌数を解析した結果、IL-33 KO マウスでは、野生型マウスに比べ有意に増加していた。その防御機構を明らかにする為に、BCG 感染マクロファージに rIL-33 を添加し NF-▪B 活性および殺菌活性を調べたところ、NF-▪B 活性および殺菌活性の増強が認められたが、iNOS の発現増強には影響は認められなかった。抗菌性ペプチドの発現は lipocalin-2 および S100A8 のみに IL-33 濃度依存的増強が認められ、CRAMP (cathelin-related antimicrobial peptide) や PLA2G2A (phospholipase A2 group IIA)の増強は認められなかった。これらのことから、マイコバクテリアの感染早期において、IL-33 介在性シグナルが抗菌性ペプチドの発現増強を誘導し、部分的に感染防御能を亢進していることを示唆している。

D. 考察

IL-17F は、IL-17A と相同性が高いにもかかわらず、IL-17A に比べてその感染防御における機能に不明な点が多い分子である。IL-17A は結核菌肺感染に対する感染防御において、成熟肉芽腫形成の誘導を介して重要な役割を担うことが報告している。一方、IL-17F は、腸管粘膜、口腔粘膜あるいは鼻粘膜における細胞外寄生性病原体感染に対する防御免疫に重要であることが報告されている。しかしながら、肺粘膜における IL-17F の役割については報告がなされていなかった。また、IL-17F と IL-17A は同じ受容体を介して刺激を伝達するが、その機能的な違いについても明確ではなかった。これらの点を解明するために、本研究では IL-17F KO マウスでの結核菌肺感染モデルにおける感染防御免疫応答を正常および IL-17A KO マウスのそれと比較検討を行った。その結果、IL-17F 発現細胞と IL-17A 発現細胞の細胞種とその空間的配置の違いが、この類似したサイトカインの役割の相違に反映される可能性が強く示唆された。

結核菌肺感染における IL-17F と IL-17A の機能的差異は、その発現細胞の違いに起因する可能性が本研究から強く示唆された。IL-17F は T 細胞などのリンパ球系細胞に加えて上皮細胞が発現するのに対して、IL-17A は主にリンパ球系の細胞により発現されることが報告されており、結核菌感染肺においても主要な IL-17A 産生細胞は TCRγδ型 T 細胞であることが明らかになっている。この TCRγδ型 T 細胞が、肉芽腫を形成するマクロファージと共局在することも組織学的に確認されている。これに対して、本研究の結果から、BCG 感染肺において IL-17F はリンパ球からほとんど産生されないことがフローサイトメトリー解析により示され、さらにⅡ型肺胞上皮細胞が主な IL-17F 産生細胞であることが病理組織学的解析から示唆された。IL-17F の恒常的発現が非感染肺の肺胞上皮でも認められており、この所見は IL-17F が病原体の侵入に対して即時に働きうる可能性を示している。ま

た、IL-17F およびその産生細胞であるII型肺胞上皮細胞は感染により誘導される肉芽腫の外側で顕著に認められたが、肉芽腫内には認められなかった。これは結核菌感染肺における IL-17F の役割を理解していく上で重要な発見であると考えられる。すなわち、感染初期では、肉芽腫内に含まれるTCRγδ型 T 細胞の産生する IL-17A と肉芽腫の周辺の II 型肺胞上皮細胞から産生される IL-17F が共同して成熟肉芽腫の形成を誘導し、結核菌の封じ込めを誘導するが、肉芽腫構造がさらに拡張する慢性期においては、IL-17F 産生細胞が肉芽腫の中心から遠ざかるために、IL-17F の影響が減弱になる可能性が考えられた。

一方、Interleukin (IL)-1 サイトカイン・ファミリーに属する IL-33 は、その受容体である ST2L と IL-1RAcP を介して、主に 2 型免疫応答を誘導することがよく知られている。IL-33 は通常、核内に存在し、ネクローシスに伴って細胞外へ放出され、IL-33 受容体（ST2/IL-1RA p）を発現する細胞を活性化する。炎症部位においては好中球などが放出するプロテアーゼによって限定分解を受け、さらに活性が上昇することが報告されている。一方、アポトーシスの場合は活性化された Caspase-3 や Caspase-7 によって IL-33 は切断され、機能性は失活する。肺では特に上皮細胞や内皮細胞から IL-33 が放出されると考えられている。IL-33 は ST2 を介して、マスト細胞、Th2 リンパ球、好塩基球、好酸球、マクロファージから炎症性または Th2 型サイトカインやケモカインを産生誘導し、アレルギー性疾患をはじめ、様々な炎症反応において重要な役割を担っている。最近、ST2KO マウスを用いた *Cryptococcus neoformans* 肺感染モデルにおいて、IL-33 介在性シグナルが自然免疫および獲得免疫応答に重要な役割を担っていることが明らかになった。一方、結核菌肺感染 ST2 KO マウスモデルにおいては、野生型マウスにおける免疫応答と変わらないことが既に報告されている。しかしながら、結核菌感染肺における IL-33 の防御機構は未だ不明瞭な点が非常に多い。本研究では IL-33 KO マウスを用い、結核菌による慢性感染に対する IL-33 の関与を検討した。結核菌感染における生存率、臓器内菌数、Th1 型免疫応答能、肉芽腫形成を比較したところ、IL-33 KO マウスは野生型マウスと差が認められなかった。このことから、結核菌の慢性感染肺での IL-33 は積極的に感染防御に関与してこないことが予想された。これは、ST2 KO マウスを用いた結核菌感染では正常な免疫応答（防御免疫）である報告と一致する。次いで、自然免疫レベルでの検討は強毒株であるヒト型結核菌（*M. tuberculosis* H37Rv）では検討しづらい故に、弱毒株である *M. bovis* BCG の肺感染モデルを用いて検討した。BCG 感染肺では、IL-33 欠損により臓器内菌数の増加（菌の排除能低下）が認められ、また IL-33 の感染マクロファージの活性化（抗菌性ペプチド発現増強）に部分的に関与する可能性が考えられた。今後、結核菌感染における IL-33 の Th1 や Tc1 免疫応答への関与を含め、より詳細な感染防御能を検討する必要があると考えられる。

E. 結論

IL-17 サイトカイン・ファミリーの一つである IL-17F は結核菌感染肺では肉芽腫の周辺の II 型肺胞上皮細胞で強く発現され、感染早期の防御免疫に参加するものと推定された。すなわち、感染早期では、肉芽腫近位の IL-17F が肉芽腫成熟を誘導し、結核菌の封じ込めに働くが、肉芽腫構造がさらに拡張する慢性感染後期では、IL-17F 産生細胞が肉芽腫の中心から遠ざかるために、IL-17F の影響が減弱になる可能性が考えられた。これらのことより、IL-17A と IL-17F の機能分担がその局在により規定される可能性が示唆された。

また、結核菌感染における IL-33 の関与に関して検討を行った。結核菌感染 ST2 KO マウスは野生型マウスにおける免疫応答と変わらないことが報告されている。しかし、我々の結果はそれに反し、弱毒マイコバクテリアである BCG 感染において IL-33 が抗

菌ペプチド産生誘導などの機構を介して、特に自然免疫レベルでの防御に関与することが示唆された。

G. 研究発表

1. 論文発表

なし

2. 学会発表

1) Umemura, M., M. Fukui, S. Touyama, C. Fukui, N. Teruya, T. Tamura, S. Nakae, Y. Iwakura, and G. Matsuzaki. Characterization and localization of IL-17F-producing cells during mycobacterial infection. 第 87 回日本細菌学会総会　2014 年 3 月　東京

2) Tamura, T., M. Umemura, and M. Makino. Effect of Peptide-25 on the induction of functional activation of cytotoxic T lymphocytes. 第 87 回日本細菌学会総会　2014 年 3 月　東京.

3) Fukui, M., M. Umemura, and G. Matsuzaki. Combined vaccination of subcutaneous BCG and intranasal HBHA with cholera toxin enhances early protective immunity against pulmonary *M. tuberculosis* infection. IMMUNOLOGY 2014™ AAI Annual Meeting, 2-6 May, 2014, Pittsburgh, Pennsylvania, USA.

4) Umemura, M., S. Touyma, M. Fukui, C. Fukui, S. Nakae, Y. Iwakura, and G. Matsuzaki. Role of IL-17 in chronic pulmonary mycobacterial infection. IMMUNOLOGY 2014™ AAI Annual Meeting, 2-6 May, 2014, Pittsburgh, Pennsylvania, USA.

5) 梅村正幸. 結核菌感染における肉芽腫形成および成熟に関与するサイトカインー特に IL-17 サイトカイン・ファミリーを中心として. 第 89 回日本結核病学会総会　2014 年 5 月　岐阜（教育講演）

6) 梅村正幸, 福井雅之, 福井知穂, 中江進, 松﨑吾朗. マイコバクテリア感染肺における IL-33 の防御機構. 第 79 回日本インターフェロン・サイトカイン学会学術集会　2014 年 6 月　札幌市

7) 梅村正幸, 福井雅之, 福井知穂, 中江進, 松﨑吾朗. IL-33 のマイコバクテリア感染防御免疫に対する増強効果. 第 25 回日本生体防御学会学術総会　2014 年 7 月　仙台市

8) 福井雅之, 梅村正幸, 松﨑吾朗. 新規抗肺結核ワクチン戦略による早期防御免疫応答の増強. 第 25 回日本生体防御学会学術総会　2014 年 7 月　仙台市

9) 松﨑吾朗, 沖田大和, 浜田聡, 梅村正幸. IL-22 が誘導するヒト Phospholipase A2 Group IIA (PLA2G2A) による *Listeria monocytogenes* 感染防御. 第 25 回日本生体防御学会学術総会　2014 年 7 月　仙台市

10) 梅村正幸, 福井雅之, 當山清悟, 山﨑雅俊, 福井知穂, 照屋 尚子, 中江進, 岩倉 洋一郎, 松﨑吾朗. マイコバクテリア感染における IL-17 サイトカイン・ファミリーの防御能. 第 67 回日本細菌学会九州支部総会　2014 年 9 月　鹿児島市

11) 福井雅之, 梅村正幸, 山﨑 雅俊, 福井知穂, 照屋 尚子, 中江進, 松﨑吾朗. マイコバクテリア感染早期におけるインターロイキン(IL)-33 の防御効果. 第 67 回日本細菌学会九州支部総会　2014 年 9 月　鹿児島市

12) 梅村正幸. 結核肺感染における interleukine-17 の関与とその応用. 第 10 回霊長類医科学フォーラム　2014 年 11 月　つくば市（招待講演）

13) Umemura, M., M. Fukui, M. Yamasaki, C. Fukui, T. Tamura, S. Nakae, and G. Matsuzaki. Involvement of IL-33 in the protective immunity against lung mycobacterial infection. 第 43 回日本免疫学会学術集会　2014 年 12 月　京都市

H. 知的財産権の出願・登録状況

1. 特許取得　　なし

2. 実用新案登録 なし
3. その他　　なし

研究成果の刊行に関する一覧表

別紙 5-1

研究成果の刊行に関する一覧表

書籍

著者氏名	論文タイトル名	書籍全体の編集者名	書　籍　名	出版社名	出版地	出版年	ページ

別紙 5-1

雑誌

発表者氏名	論文タイトル名	発表誌名	巻号	ページ	出版年
T. Sekizuka, M. Kai, K. Nakanaga, N. Nakata, Y. Kazumi, S. Maeda, M. Makino, Y. Hoshino, M. Kuroda.	Complete Genome Sequence and Comparative Genomic Analysis of *Mycobacterium massiliense* JCM 15300 in the *Mycobacterium abscessus* Group Reveal a Conserved Genomic Island MmGI-1 Related to Putative Lipid Metabolism.	PLoS ONE	in press		2014
S. Mori, H. Kim, E. Rimbara, Y. Arakawa, K. Shibayama.	Roles of Ala-149 in the catalytic activity of diadenosine tetraphosphate phosphorylase from *Mycobacterium tuberculosis* H37Rv.	Biosci. Biotechnol. Biochem.	in press		2014
H. Kim, K. Shibayama, E. Rimbara, S. Mori	Biochemical characterization of quinolinic acid phosphoribosyltransferase from *Mycobacterium tuberculosis* H37Rv and inhibition of its activity by pyrazinamide.	PLoS ONE	9(6)	e100062	2014
T. Mukai, Y. Tsukamoto, Y. Maeda, T. Tamura, M. Makino.	Efficient Activation of Human T Cells of Both CD4 and CD8 Subsets by Urease Deficient-Recombinant BCG that Produced Heat Shock Protein 70-*Mycobacterium tuberculosis*-Derived Major Membrane Protein-II Fusion Protein.	Clin. Vaccine Immunol.	21	1-11	2014
Y. Tsukamoto, Y. Maeda, T. Tamura, T. Mukai, M. Makino.	Polyclonal activation of naïve T cells by urease deficient-recombinant BCG that produced protein complex composed of heat shock protein 70, CysO and major membrane protein-II.	BMC Infect. Dis.	14	179	2014

Y. Tsukamoto, Y. Maeda, M. Makino.	Evaluation of major membrane protein-I as a serodiagnostic tool of pauci-bacillary leprosy.	Diagn. Microbiol. Infect. Dis.	80	62-65	2014
M. S. Duthie, R. N. Coler, J. D. Laurance, L. H. Sampaio, R. M. Oliveira, A. L. Sousa, M. M. Stefani, Y. Maeda, M. Matsuoka, M. Makino, S. G. Reed.	Protection against *M. leprae* infection by the ID83/GLA-SE and ID93/GLA-SE vaccines developed for tuberculosis.	Infect. Immun.	82	3979-3985	2014
K. Nakanaga, T. Sekizuka, H. Fukano, Y. Sakakibara, F. Takeuchi, S. Wada, N. Ishii, M. Makino, M. Kuroda, Y. Hoshino.	Discrimination of *Mycobacterium abscessus* subsp. *massiliense* from *Mycobacterium abscessus* subsp. *abscessus* in Clinical Isolates by Multiplex PCR.	J. Clin. Microbiol.	52	251-259	2014
R. Yang, C. Xi, D. R. Sita, S. Sakai, K. Tsuchiya, H. Hara, Y. Shen, H. Qu, R. Fang, M. Mitsuyama I. Kawamura	The RD1 locus in the *Mycobacterium tuberculosis* genome contributes to the maturation and secretion of IL-1α from infected macrophages through the elevation of cytoplasmic calcium levels and calpain activation.	Pathog. Dis.	70	51-60	2014
K. Ohtsuka, H. Ohnishi, E. Nozaki, J. Pais Ramos, E. Tortoli, S. Yonetani, S. Matsushima, Y. Tateishi, S. Matsumoto, T. Watanabe.	Whole-Genome Sequence of *Mycobacterium kyorinense*.	Genome Announc.	2	e01062-01014	2014

Y. Nishiuchi, A. Tamaru, Y. Suzuki, S. Kitada, R. Maekura, Y. Tateishi, M. Niki, H. Ogura, S. Matsumoto.	Direct detection of *Mycobacterium avium* in environmental water and scale samples by loop-mediated isothermal amplification.	J. Water Health.	12	211-219	2014
Y. Fujii, S. Kaneko, S. M. Nzou, M. Mwau, S. M. Njenga, C. Tanigawa, J. Kimotho, A. W. Mwangi, I. Kiche, S. Matsumoto, M. Niki, M. Osada-Oka, Y. Ichinose, M. Inoue, M. Itoh, H. Tachibana, K. Ishii, T. Tsuboi, L. M. Yoshida, D. Mondal, R. Haque, S. Hamano, M. Changoma, T. Hoshi, K. Kamo, M. Karama, M. Miura, K. Hirayama.	Serological surveillance development for tropical infectious diseases using simultaneous microsphere-based multiplex assays and finite mixture models.	PLoS Negl. Trop. Dis.	8	e3040	2014

PLOS | ONE

Biochemical Characterization of Quinolinic Acid Phosphoribosyltransferase from *Mycobacterium tuberculosis* H37Rv and Inhibition of Its Activity by Pyrazinamide

Hyun Kim, Keigo Shibayama, Emiko Rimbara, Shigetarou Mori*

Department of Bacteriology II, National Institute of Infectious Diseases, Musashi-Murayama, Tokyo, Japan

Abstract

Quinolinic acid phosphoribosyltransferase (QAPRTase, EC 2.4.2.19) is a key enzyme in the *de novo* pathway of nicotinamide adenine dinucleotide (NAD) biosynthesis and a target for the development of new anti-tuberculosis drugs. QAPRTase catalyzes the synthesis of nicotinic acid mononucleotide from quinolinic acid (QA) and 5-phosphoribosyl-1-pyrophosphate (PRPP) through a phosphoribosyl transfer reaction followed by decarboxylation. The crystal structure of QAPRTase from *Mycobacterium tuberculosis* H37Rv (MtQAPRTase) has been determined; however, a detailed functional analysis of MtQAPRTase has not been published. Here, we analyzed the enzymatic activities of MtQAPRTase and determined the effect on catalysis of the anti-tuberculosis drug pyrazinamide (PZA). The optimum temperature and pH for MtQAPRTase activity were 60°C and pH 9.2. MtQAPRTase required bivalent metal ions and its activity was highest in the presence of Mg^{2+}. Kinetic analyses revealed that the K_m values for QA and PRPP were 0.08 and 0.39 mM, respectively, and the k_{cat} values for QA and PRPP were 0.12 and 0.14 [s^{-1}], respectively. When the amino acid residues of MtQAPRTase, which may interact with QA, were substituted with alanine residues, catalytic activity was undetectable. Further, PZA, which is an anti-tuberculosis drug and a structural analog of QA, markedly inhibited the catalytic activity of MtQAPRTase. The structure of PZA may provide the basis for the design of new inhibitors of MtQAPRTase. These findings provide new insights into the catalytic properties of MtQAPRTase.

Citation: Kim H, Shibayama K, Rimbara E, Mori S (2014) Biochemical Characterization of Quinolinic Acid Phosphoribosyltransferase from *Mycobacterium tuberculosis* H37Rv and Inhibition of Its Activity by Pyrazinamide. PLoS ONE 9(6): e100062. doi:10.1371/journal.pone.0100062

Editor: Beata G. Vertessy, Institute of Enzymology of the Hungarian Academy of Science, Hungary

Received November 13, 2013; **Accepted** May 22, 2014; **Published** June 20, 2014

Funding: This study was supported, in part, by a grant from the Ministry of Health, Labor, and Welfare of Japan (H24-Shinkou-Ippan-010) and by a Grant-in-Aid for Young Scientists (No. 25860329) from the Ministry of Education, Culture, Sports, Science, and Technology of Japan. The funders had no role in study design, data collection and analysis, decision to publish, or preparation of the manuscript.

Competing Interests: The authors have declared that no competing interests exist.

* Email: mshige@niid.go.jp

Introduction

Tuberculosis (TB) is a chronic infectious disease, caused by the intracellular pathogen *Mycobacterium tuberculosis*, with an estimated 8.7 million cases and 1.4 million deaths each year according to a 2012 World Health Organization (WHO) Report [1]. The emergence of resistance to anti-TB drugs, in particular multi-drug-resistant TB (MDR-TB), is a public health problem and poses a serious threat to global control of TB [2–4]. Therefore, there is an urgent need for new countermeasures against TB. To address this issue, the aim of the present study was to define the functions of poorly characterized enzymes that may provide targets for designing new drugs to eradicate *M. tuberculosis* infections.

Quinolinic acid phosphoribosyltransferase (QAPRTase; EC 2.4.2.19) is encoded by *nadC* and is a key enzyme in the *de novo* pathway of nicotinamide adenine dinucleotide (NAD) biosynthesis [5–7]. NAD is a coenzyme of pivotal importance in maintaining redox balance and energy metabolism and is continuously interconverted between oxidized (NAD) and reduced (NADH) forms [8]. In most bacteria, NAD biosynthesis is essential for cell survival and viability [9], which makes it an attractive target for the development of new antibacterial drugs, with steps shared by *de novo* and recycling pathways as a source of candidate enzymes for therapeutic intervention [5,10–12].

QAPRTase catalyzes the Mg^{2+}-dependent transfer of the phosphoribosyl moiety from 5-phosphoribosyl-1-pyrophosphate (PRPP) to the nitrogen atom of quinolinic acid (QA) to generate nicotinic acid mononucleotide (NAMN), pyrophosphate (PPi), and CO_2 (Fig. 1) [5,13–15]. QA is the first intermediate in the *de novo* pathway of NAD biosynthesis that is common to all organisms and is mainly produced by the degradation of tryptophan in most eukaryotes [5,16,17]. In contrast, in prokaryotes, including *M. tuberculosis*, it is produced from L-aspartate and dihydroxyacetone phosphate by the enzymes encoded by *nadA* (quinolinic acid synthetase) and *nadB* (L-aspartate oxidase) [18,19]. In *M. tuberculosis*, *nadA*, *nadB*, and *nadC* are encoded in a single operon (*nadABC*) which is regulated by a repressor encoded by *nadR* [5,20].

QAPRTase is a member of the phosphoribosyltransferase (PRTase) family of enzymes, which catalyzes the formation of nucleotides from nitrogenous bases and their common substrate PRPP [7,13,21]. PRTases are classified into four subclasses (types I, II, III, and IV) according to their structures [15,22–26].

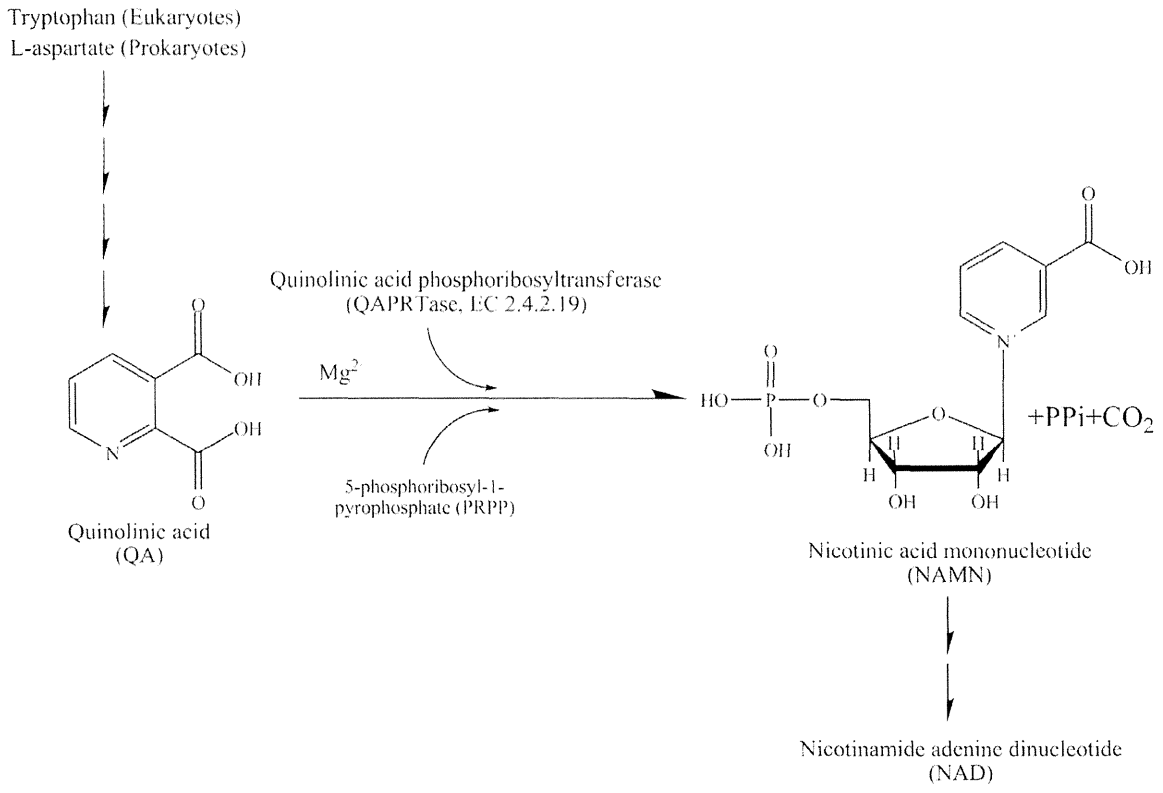

Figure 1. Schematic representation of the reaction catalyzed by QAPRTase.
doi:10.1371/journal.pone.0100062.g001

QAPRTase is a type II PRTase that participates in the *de novo* pathway of the pyridine coenzyme NAD [7,15]. Recently, nicotinic acid phosphoribosyltransferase (NAPRTase) and nicotinamide phosphoribosyltransferase, which are involved in the salvage pathways of NAD biosynthesis, have been classified as type II PRTases [15,23,24,27]. The activities of QAPRTase and NAPRTase were similar, although they are specific for their respective substrates [28,29]. *M. tuberculosis* relies entirely on the *de novo* pathway of NAD for survival; therefore, it should be extremely vulnerable to drugs targeted against QAPRTase. The crystal structure of QAPRTase from *M. tuberculosis* (MtQAPRTase) is known [5]; however, the biochemical properties of MtQAPRTase remain to be determined. Therefore, in the present study, we examined and characterized the enzymatic activities of MtQAPRTase.

QA is a structural analog of the anti-tuberculosis prodrug pyrazinamide (PZA), and pyrazinoic acid (POA) is its active form. PZA is an important component of first line anti-TB drugs in the chemotherapy for TB and MDR-TB [30,31]. Mycobacteria acquire resistance to PZA through mutations in the gene encoding pyrazinamidase (PZase), an enzyme that converts PZA to the active anti-bacterial form of POA [30,32,33]. Although mutations in PZase (encoded by *pncA*) responsible for the generation of most PZA-resistant *M. tuberculosis* strains have been identified [9], some PZA-resistant *M. tuberculosis* strains do not harbor *pncA* mutations [33]. The mechanism of action and main target of PZA are still not clearly understood; however, intensive investigations are in progress across laboratories worldwide [30–34]. Recently, Shi W. *et al.* [31] reported that the PZA inhibits trans-translation in *M. tuberculosis*, and suggest that POA binds to ribosomal protein S1 (RpsA) and subsequently inhibits trans-translation. Therefore, PZA may have interfered with bacterial growth and survival.

Because PZA and POA are structural analogs of QA, we reasoned that MtQAPRTase may use PZA or POA as a substrate, or these substrates may inhibit the enzymatic activity of MtQAPRTase.

In the present study, we examined and characterized the enzymatic activities of wild type (WT) plus mutant MtQAPRTases and the effect of PZA and POA on WT MtQAPRTase *in vitro*.

Materials and Methods

Materials

Pyrazinoic acid (POA), nicotinic acid mononucleotide (NAMN), 2,3-pyridinedicarboxylic acid (QA), and 5-phosphoribosyl-1-pyrophosphate (PRPP) were purchased from Sigma-Aldrich (Castle-Hill, Australia). Pyrazinamide (PZA) was from Tokyo Kasei Kogyo (Tokyo, Japan). Ammonium dihydrogen phosphate, t-butyl ammonium hydrogen sulfate, isopropyl β-D-1-thiogalactopyranoside (IPTG), ampicillin, and kanamycin were purchased from Wako Pure Chemicals Ltd (Tokyo, Japan). The TOPO TA cloning kit (pCR 4-TOPO) was purchased from Life Technologies (Carlsbad, CA) and used for cloning and nucleotide sequencing. The BCA protein assay kit, pH range 2.2–11.0 stock option pH buffer kit, and gel-filtration calibration kit were from Fisher Thermo Scientific (Pierce, Rockford, IL), Hampton Research (Aliso Viejo, CA) and GE Healthcare Bio-Sciences (Buckingham-

Table 1. PCR primers.

Primer NO.	Sequence of oligonucleotide (Positions)	Comments
K-001	5′—CCC*ATATG*GGGGTTATCCGACTGGG—3′ (1–19)	WT *nadC*
K-003	5′—GG*AAGCTT*CTAATGATGATGATGATGATGCATATCCAAGCCGATGTC—3′ (838–858)	WT *nadC*
K-006	5′—CAACATGGTGGCCTCGGCGGTC—3′ (303–324)	Arg105Ala-Rv-*nadC*
K-007	5′—CCGCCGAGGCCACCATGTTGAAC—3′ (305–327)	Arg105Ala-Fw-*nadC*
K-008	5′—CAGCGTCTTAGCGGTATCGC—3′ (406–426)	Arg139Ala-Rv-*nadC*
K-009	5′—CGCGATACCGCTAAGACGCTGC—3′ (405–427)	Arg139Ala-Fw-*nadC*
K-010	5′—CCCAACCCCAGCGCATGGTTGAC—3′ (474–497)	Arg162Ala-Rv-*nadC*
K-011	5′—CGTCAACCATGCGCTGGGGTTGG—3′ (473–427)	Arg162Ala-Fw-*nadC*
K-012	5′—CGTGGTTGTCCGCGATTAGCGC—3′ (504–526)	Lys172Ala-Rv-*nadC*
K-013	5′—CGCGCTAATCGCGGACAACCACG—3′ (503–526)	Lys172Ala-Fw-*nadC*

Mutated codons are shown in bold type.
Restriction endonuclease cleavage sites and 6xHis are written in italics and underlined, respectively.
doi:10.1371/journal.pone.0100062.t001

shire, UK), respectively. Restriction endonucleases were purchased from New England BioLabs, Inc. (Ipswich, MA).

Bacterial strains and plasmid

Escherichia coli strain DH5α (Life Technologies) was used as the host for molecular cloning. *E. coli* strain BL21 (DE3) was purchased from Merck KGaA (Darmstadt, Germany) and used for protein expression. The pET-30a plasmid (Merck KGaA) was used construct in an expression vector to produce WT and mutant versions of recombinant MtQAPRTase.

Cloning and mutagenesis of *nadC* from *M. tuberculosis* H37Rv genomic DNA

Genomic DNA from *M. tuberculosis* H37Rv was isolated as previously described [35,36]. The *nadC* (Rv1596, accession number; NP_216112.1) of *M. tuberculosis* H37Rv was amplified from genomic DNA [20] by using the polymerase chain reaction (PCR). The reaction mixture (20 μL) contained long and accurate (LA) PCR buffer II (Mg^{2+}-free); 2.5 mM $MgCl_2$; 200 μM each of dATP, dCTP, dGTP, and dTTP; 250 ng of genomic DNA from *M. tuberculosis* H37Rv; 1.25 units of LA Taq DNA polymerase (all from TaKaRa Bio, Kyoto, Japan); and 0.1 μM of each primer. The primers are shown in Table 1. PCR was conducted using a Takara PCR Thermal Cycler Dice Mini (TaKaRa Bio Inc., Shiga, Japan) as follows: pre-denaturation at 98°C for 2 min, 35 cycles of denaturation at 98°C for 10 sec, annealing at 55°C for 10 sec and extension at 72°C for 2 min, and final extension at 72°C for 2 min. K-001 and K-003 primers were used to amplify WT *nadC* (Table 1). Nucleotide sequences encoding a 6x-histidine residue cluster were added directly upstream of the *nadC* stop codon on C-terminal. The PCR product (885 bp) was ligated to the TA cloning plasmid and used to transform *E. coli* DH5α. The recombinant *nadC* plasmid DNA was recovered from the colonies and digested with *Nde*I and *Xho*I. The *nadC* product was ligated to pET-30a expression vector that was digested with the same restriction endonucleases. Mutant *nadC* genes were generated from WT *nadC* by using a QuikChange Site-Directed Mutagenesis Kit (Agilent Technologies, Inc., Santa Clara, CA) according to the manufacturer's instruction. The list of primers used to generate mutants is shown in Table 1. After mutagenesis, plasmids were recovered and purified using a Promega Minipreps DNA purification kit (Madison, WI, USA). WT and mutant plasmids were confirmed by sequencing with ABI Prism BigDye Terminator v3.1 Cycle Sequencing kit (Life Technologies). The sequencing reactions were performed according to the manufacturer's instructions. The sequencing products were analyzed using an ABI Prism 3130*xl* Genetic Analyzer (Life Technologies). The sequences generated by the software were compared with their respective *nadC* sequence using Bioedit software (http://www.mbioedit.com/). Using the molecular modeling program MOE (Molecular Operating Environment, Chemical Computing Group, Montreal, Canada), we constructed a few models, which were elongated by six histidines at the C-terminus. These models were generated and structure energies were minimized using CHARMM27 force field (gradient below 0.5); the resulting structures were used as starting conformations for molecular dynamics simulations (MD) for 100 ps at 300 K. During the simulation, all amino acid residues were flexible.

Expression and purification of MtQAPRTase WT and mutants

WT and mutant forms of MtQAPRTase were purified as described previously [35,37] with the following modifications. *E. coli* BL21 (DE3) was transformed with expression vectors carrying the *M. tuberculosis* WT or mutant *nadC*. Single colonies were picked and grown overnight at 37°C in 4 mL of Luria-Bertani (LB) medium containing 50 μg/mL kanamycin. Overnight cultures (2 mL) were used to inoculate 200 mL of LB medium containing kanamycin. Cells were then cultured at 37°C for 5 h, until the optical density (OD) at 600 nm reached 0.8 to 1.0. Expression of recombinant enzymes was induced with 1 mM IPTG, followed by incubation at 14°C for 18 h. The bacteria were harvested by centrifugation at 13,000×*g* at 4°C for 10 min, the pellets were stored at −80°C for 12 h, then suspended in 7 mL of binding buffer (20 mM sodium phosphate [pH 7.4], 0.5 M NaCl, 40 mM imidazole), and disrupted by sonication at 80% pulsar power, 40 sec on/1 min off 10-times on ice, using a UP50H sonicator (Hielscher Ultrasonic, Teltow, Germany). The extracts were centrifuged at 13,000×*g* at 4°C for 10 min, and the supernatants were harvested. The cell extracts were injected onto a HisTrap HP column (1.6×2.5 cm; GE Healthcare Bio-Sciences, Buckinghamshire, UK) pre-equilibrated with deionized water and binding buffer. The columns were washed with binding buffer until the absorbance reached a steady baseline, and the proteins were eluted using an elution buffer containing 20 mM sodium phosphate (pH 7.4), 0.5 M NaCl, and 0.5 M imidazole. The

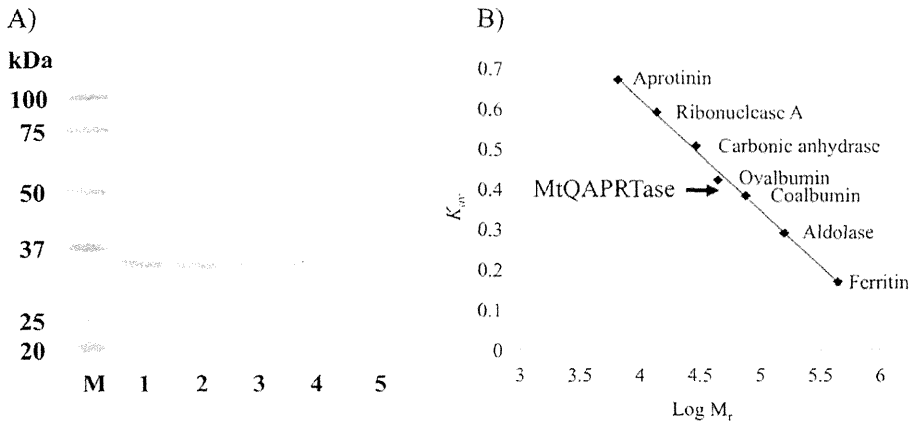

Figure 2. SDS-PAGE analysis and determination of the molecular mass of recombinant MtQAPRTases. A) The WT and mutant enzymes are shown above the designated lane. Approximately 5 μg of each protein was loaded on a 5–20% SDS-polyacrylamide gel. Lane M, protein size markers; lane 1, WT MtQAPRTase; lane 2, Arg105′-Ala; lane 3, Arg139Ala; lane 4, Arg162Ala; and lane 5, Lys172Ala. B) Estimation of the molecular mass of recombinant MtQAPRTase using Superdex 200 gel-filtration chromatography. The elution position of MtQAPRTase is indicated by an arrow. Protein standards were as follows: aprotinin (6.5 kDa); ribonuclease A (13.7 kDa); carbonic anhydrase (29.0 kDa); ovalbumin (44.0 kDa); conalbumin (75.0 kDa); aldolase (158.0 kDa), and ferritin (440.0 kDa). K_{av} values were calculated using the following equation: $K_{av} = (V_e - V_o)/(V_c - V_o)$ is the column void volume, V_e is the elution volume, and V_c is the geometric column volume. The V_o value used was the V_e of Blue Dextran 2000. M_r indicates the molecular weight.
doi:10.1371/journal.pone.0100062.g002

eluted proteins were concentrated using an Amicon Ultra-15 (Millipore, Billerica, MA) for 20 min at 4°C. WT and mutants MtQAPRTase were further purified using a Hi-Load 16/60 Superdex 200 prep grade column (GE Healthcare Bio-Sciences) in 10 mM sodium phosphate (pH 7.4), 50 mM NaCl buffer, and buffer exchange was performed to remove imidazole from the elutes with the same buffer. Based on the gel-filtration chromatography results, the eluted peak samples were assayed for QAPRTase activity and were analyzed using sodium dodecyl sulfate-polyacrylamide gel electrophoresis (SDS-PAGE). Protein concentrations were determined using a BCA Protein Assay kit.

QAPRTase assay and characterization of MtQAPRTase activity

MtQAPRTase WT and mutant enzyme activities were determined by quantifying substrates using a high-performance liquid chromatography system (HPLC, Shimadzu, Kyoto, Japan) according to previously described methods with modifications [16,35,38,39]. The HPLC system comprised a Prominence UV/VIS detector and a 4.6×250 mm COSMOSIL PACKED 5C18 AR-II column (Nacalai Tesque, Inc., Kyoto, Japan). Reaction mixtures contained 50 mM KH_2PO_4 (pH 7.2), 6 mM $MgCl_2$, 1.5 mM QA, 1 mM PRPP, and 1.62 μM of purified WT or mutant MtQAPRTase in a total volume of 100 μL, and were then incubated at 37°C for 30 min; the reaction was stopped by heating at 98°C for 3 min, and then the reaction mixtures were centrifuged at 13,000×*g* for 5 min. The supernatants (100 μL) were subjected to HPLC analysis using a column equilibrated with deionized water. The adsorbed products such as QA, PRPP, and NAMN, were eluted with a gradient of water and HPLC buffer (0.02 M t-butyl ammonium hydrogen sulfate and 0.2 M dihydrogen phosphate [pH 5.3]) at a flow rate of 0.6 mL/min, and products were detected by their absorbance at 270 nm. One unit (U) of enzyme activity was defined as the 1.0 μmol of NAMN in 1 min at 37°C. The effects of pH on enzyme activity were determined using citric acid anhydrous (pH 2.2 and 3.2), sodium acetate trihydrate (pH 4.2), TRIS-sodium citrate dehydrate (pH 5.2), cacodylic acid sodium salt trihydrate (pH 6.2), sodium 4-(2-hydroxyethyl)-1-piperazineethanesulfonic acid (pH 7.2), trihydrochloride (pH 8.2), and 3-(cyclohexylamino)-2-hydroxy-1-propane sulfonic acid (pH 9.2, 10.2, and 11.2). To determine the temperature optimum, QAPRTase activities were measured over the range of 20−70°C in 50 mM KH_2PO_4 (pH 7.2) for 30 min. The effects of divalent cations on QAPRTase activity were determined using reaction mixtures containing 6 mM each of Mg^{2+} ($MgCl_2$), Mn^{2+} ($MnCl_2$), Co^{2+} ($CoCl_2$), Fe^{2+} ($FeCl_2$), Ca^{2+} ($CaCl_2$), Zn^{2+} ($ZnCl_2$), and Cu^{2+} ($CuSO_4$). Enzyme analyses were performed in triplicate to determine reproducibility.

Kinetic parameters of MtQAPRTase

The kinetic parameters of recombinant MtQAPRTase activities were performed by a monitoring spectrophotometric assay using Ultrospec 3000 UV/Visible Spectrophotometer (GE Healthcare Biosciences, Buckinghamshire, UK). Typical assay mixtures contained 50 mM KH_2PO_4 (pH 7.2), 6 mM $MgCl_2$, various concentration of QA (0.02–0.4 mM), PRPP (0.02–1.5 mM), and 1.62 μM of purified WT MtQAPRTase in a total volume of 100 μL. A spectrophotometric assay of QAPRTase activity over 20 min at 37°C measured the increase in absorbance at 266 nm resulting from the conversion of QA to NAMN ($\Delta A266 = 920\ M\ cm^{-1}$) [16,39]. Ultrospec 3000 UV/Visible Spectrophotometer plotted the increase in absorbance at 266 nm (dA) against time (min) and calculated the initial slope (dA/min) automatically. The initial velocity was calculated from the slope (dA/min). The reaction mixtures for determination of K_m values from initial velocity data were prepared using various concentrations of PRPP and a fixed concentration of QA (0.3 mM); conversely, reaction mixtures were also prepared using various concentrations of QA and a fixed concentration of PRPP (1.0 mM). The reaction was initiated by the addition of WT MtQAPRTase, and absorbance was immediately estimated. To determine K_m and k_{cat} values when using QA and PRPP as substrates, their concentrations were varied. Kinetic parameters for MtQAPRTase activity were calculated using GraphPad Prism 5 software (GraphPad Software,

Table 2. Purification of recombinant QAPRTase from *M. tuberculosis* H37Rv.

Purification Step	Total Protein (mg)	Total activity (Unit)	Yield (%)	Specific activity (Unit/mg)	Purification (fold)
Cell extract	481.8	91.5	100	0.2	1.0
His-Trap	34.3	62.7	68	1.8	9.6
Sephacryl S-200	14.0	17.1	19	1.2	6.4

doi:10.1371/journal.pone.0100062.t002

La Jolla, CA). Values of K_m and k_{cat} are represented as mean ± standard error of three independent determinations.

Inhibitory effects of PZA/POA and determination of IC_{50} values

The inhibitory effects of PZA and POA on MtQAPRTase activity were determined by quantifying substrates using a HPLC analysis. Reaction mixtures (100 μL) containing 6 mM $MgCl_2$, 1.5 mM QA, 1 mM PRPP, 1 mM of PZA or POA, and 1.62 μM of purified WT MtQAPRTase were incubated at pH 6.2 or 7.2 in 50 mM KH_2PO_4 buffer at 37°C for 30 min. Additionally, the drug concentrations required to inhibit the QAPRTase activity by 50% (IC_{50} values) were determined from the concentration of NAMN generated at various concentrations of PZA (0.07–0.7 mM at pH 7.2 and 0.2–2.0 mM at pH 6.2) or POA (0.5–5.0 mM at pH 7.2 and 2.0–40.0 mM at pH 6.2). IC_{50} values were represented as mean ± standard error of three independent determinations.

Determination of the molecular mass of MtQAPRTase

The molecular mass of purified MtQAPRTase was estimated using a Superdex 200 10/300GL (10×300 mm) (GE Healthcare Bio-Sciences) gel-filtration chromatography column with low- and high-molecular-weight (LMW, HMW) calibration kits (GE Healthcare Bio-Sciences) as recommended by the manufacturer. The protein standards and molecular masses were as follows: ferritin (440.0 kDa), aldolase (158.0 kDa), conalbumin (75.0 kDa), ovalbumin (44.0 kDa), carbonic anhydrase (29.0 kDa), ribonuclease A (13.7 kDa), and aprotinin (6.5 kDa).

Molecular docking study

The molecular docking and visualization studies were performed using MF mypresto v1.2 (Fiatlux Corporation, Tokyo, Japan) molecular modeling software. Coordinates of MtQAPRTase for structure-based molecular modeling were retrieved from the Protein Data Bank (PDB), USA (http://www.rcsb.org/pdb/), under the accession code [PDB ID: 1QPQ] [5]. The molecular docking models used dimeric forms of A and B subunits from the three-dimer form of MtQAPRTase and the coordinates of ligands and waters were manually removed. On the basis of the information regarding the QA-binding site, the location and size of the receptor pocket were set (Center: X: -15.796 Y: 42.865 Z: 17.445, and radius: 4 angstrom). Optional parameters in MF mypresto v1.2 were used to create a topology file, which included addition of hydrogen atoms, calculation of a grid potential, and docking simulation. Flexible docking method was used and the scores are expressed as a sum of five potentials: accessible surface area, coulomb potential, hydrogen bonds, hydrogen bond considering anisotropy, and van der Waals interactions. The protein-ligand binding free energies were estimated by MF mypresto v1.2. The results of molecular docking were visualized, and the distance between residues of amino acid and PZA was calculated using PyMOL v1.3 (http://www.pymol.org/) and WinCoot-0.7.2 (http://www.ysbl.york.ac.uk/).

Results

Expression and purification of MtQAPRTase

Full-length *nadC* from *M. tuberculosis* H37Rv was inserted into the expression vector pET-30a downstream of the T7 promoter to express a His-tagged recombinant MtQAPRTase. We confirmed

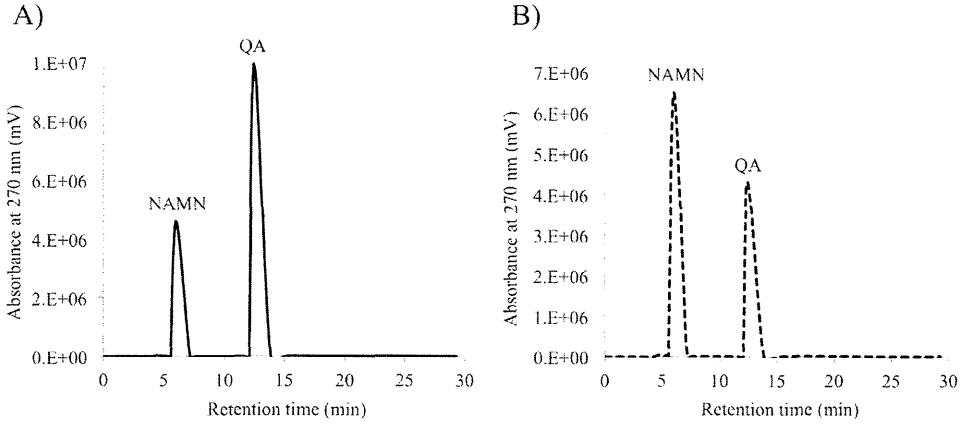

Figure 3. HPLC analysis of substrates and products. The enzymatic activities of MtQAPRTase were determined using QAPRTase assays with PRPP as the substrate in the absence (A) and presence (B) of purified recombinant MtQAPRTase. NAMN and QA eluted at 6.0 and 12.5 min.
doi:10.1371/journal.pone.0100062.g003

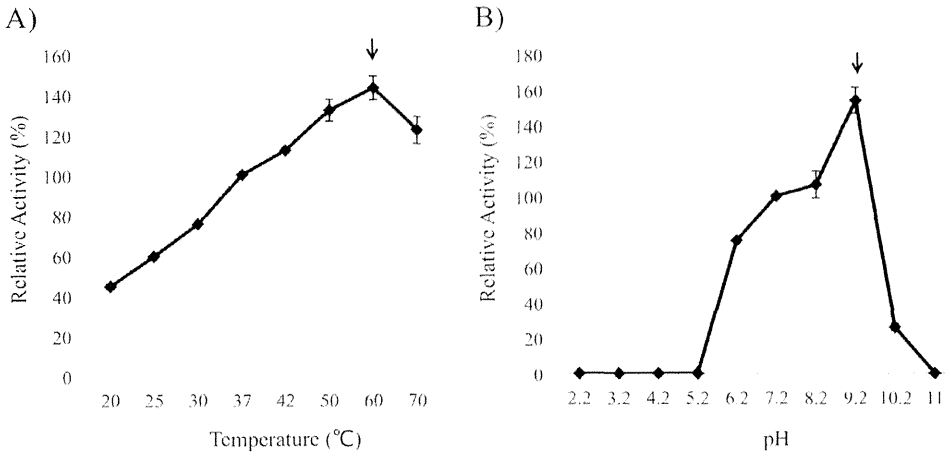

Figure 4. Temperature and pH optima. MtQAPRTase was incubated at the various temperatures (A) and at pH 2.2–11.0 (B) for 30 min. The optimum level of MtQAPRTase activity is denoted with arrows.
doi:10.1371/journal.pone.0100062.g004

the association between the location of His-tag and active site of MtQAPRTase by using MOE. This analysis shows that the His-tag could be located outside the active site of MtQAPRTase (Fig. S1), suggesting that the His-tag does not interfere with the activity of MtQAPRTase. Furthermore, it was confirmed that His-tag could not affect the multimerization of MtQAPRTase (Fig. S1). DNA sequence analysis of the recombinant plasmid confirmed the identity and integrity of *nadC* and verified that no mutations were introduced during PCR amplification. Recombinant MtQAPRTase was purified to homogeneity using a two-step column chromatographic procedure described in Materials and Methods. The molecular mass of recombinant MtQAPRTase determined using SDS-PAGE was 31 kDa (Fig. 2A, lane 2), consistent with that calculated from the amino acid sequence containing six histidine residues (30773.9 Da). The specific activity of purified recombinant MtQAPRTase was 1.2 U/mg with a yield of 19% and purification of 6.4-fold (Table 2). The molecular mass of MtQAPRTase as estimated using gel-filtration chromatography column was approximately 58 kDa (Fig. 2B), indicating that the enzyme exists as a dimer in solution.

Enzymatic activities of MtQAPRTase

The enzymatic activities of MtQAPRTase were determined using HPLC (Fig. 3). QA and NAMN were observed at 6.0 and 12.5 min, respectively (Fig. 3A), while a peak of PRPP was not detected using our separation conditions. When MtQAPRTase was added to a reaction mixture, the area of the QA and NAMN peaks decreased and increased, respectively (Fig. 3B). We then confirmed that recombinant MtQAPRTase converts QA and PRPP to NAMN, PP_i, and CO_2 in the presence of Mg^{2+}.

The optimum temperature of MtQAPRTase was 60°C, and its activity was decreased at 70°C (Fig. 4A). Its pH optimum was 9.2, and its activity could not be detected at pH values below 5.2 and above 11.0 (Fig. 4B).

QAPRTase isolated from *M. tuberculosis*, *E. coli*, and *Salmonella typhimurium* requires Mg^{2+} for activity [12,15,18]. Similarly, MtQAPRTase activity requires bivalent metal ions such as Mg^{2+}. Activity was highest in the presence of Mg^{2+} (Table 3). The relative activities of MtQAPRTase in the presence of 6 mM metal ions are shown in Table 3.

Kinetic parameters of WT MtQAPRTase

The Michaelis–Menten plot was used to estimate K_m and k_{cat} according to the activity at different concentrations of PRPP

Table 3. Effects of bivalent metal ions on QAPRTase activity.

Bivalent Metal Ions (6 mM)	Specific activity (Unit/mg)	Relative Activity (%)
Mg^{2+} ($MgCl_2$)	1.32	100
Mn^{2+} ($MnCl_2$)	0.35	27
Co^{2+} ($CoCl_2$)	0.15	12
Fe^{2+} ($FeCl_2$)	0.06	6
Ca^{2+} ($CaCl_2$)	0	0
Zn^{2+} ($ZnCl_2$)	0	0
Cu^{2+} ($CuSO_4$)	0	0
None[a]	0	0

[a]absence of metal ions.
doi:10.1371/journal.pone.0100062.t003

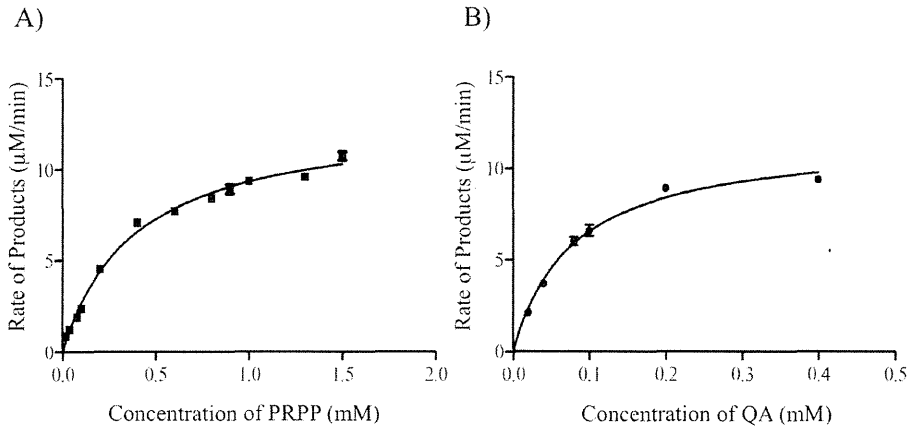

Figure 5. Kinetic studies of MtQAPRTase. The Michaelis–Menten plots for enzyme activity were generated in the presence of different concentrations of PRPP (A) and QA (B) as shown in the figure. Reaction mixtures (50 mM KH_2PO_4 [pH 7.2], 6 mM $MgCl_2$, various concentrations of QA or PRPP, and 1.62 μM of MtQAPRTase) were incubated at 37°C over 20 min. Kinetic studies were performed using reaction mixtures that contained various concentrations of PRPP and a fixed concentration of QA (0.3 mM) as the substrate; conversely, kinetic studies were also performed using reaction mixtures that contained various concentrations of QA and a fixed concentration of the PRPP (1.0 mM) as the substrate. Standard error for three independent experiments is indicated by the bars.
doi:10.1371/journal.pone.0100062.g005

(between 0.02 and 1.5 mM) and QA (between 0.02 and 0.4 mM) as substrates (Fig. 5). The K_m and k_{cat} values for PRPP were 0.39±0.03 mM and 0.14±0.30 [s^{-1}], respectively (Fig. 5A). In contrast, the K_m and k_{cat} values for QA were 0.08±0.014 mM and 0.12±0.4 [s^{-1}], respectively (Fig. 5B).

Site-directed mutagenesis and activities of mutant MtQAPRTases

X-ray crystallographic studies of QAPRTase indicate that Arg105′, Arg139, Arg162, Lys172, and His175 are located in the QA-binding site of MtQAPRTase (Fig. 6) [5,13–15,40]. Arg105′ is present in another subunit. To determine whether these residues play an important role in the enzymatic activity of MtQAPRTase, we constructed, expressed, and purified the following MtQAPRTase-single mutants: Arg105′Ala, Arg139Ala, Arg162Ala, Lys172Ala, and His175Ala (Fig. 2A and 6). The catalytic activities of the MtQAPRTase mutants could not be detected when purified preparations were evaluated at variable concentrations up to 38.9 μM, which was more than 24-fold higher than normal condition (1.62 μM). Therefore, these results indicate that these

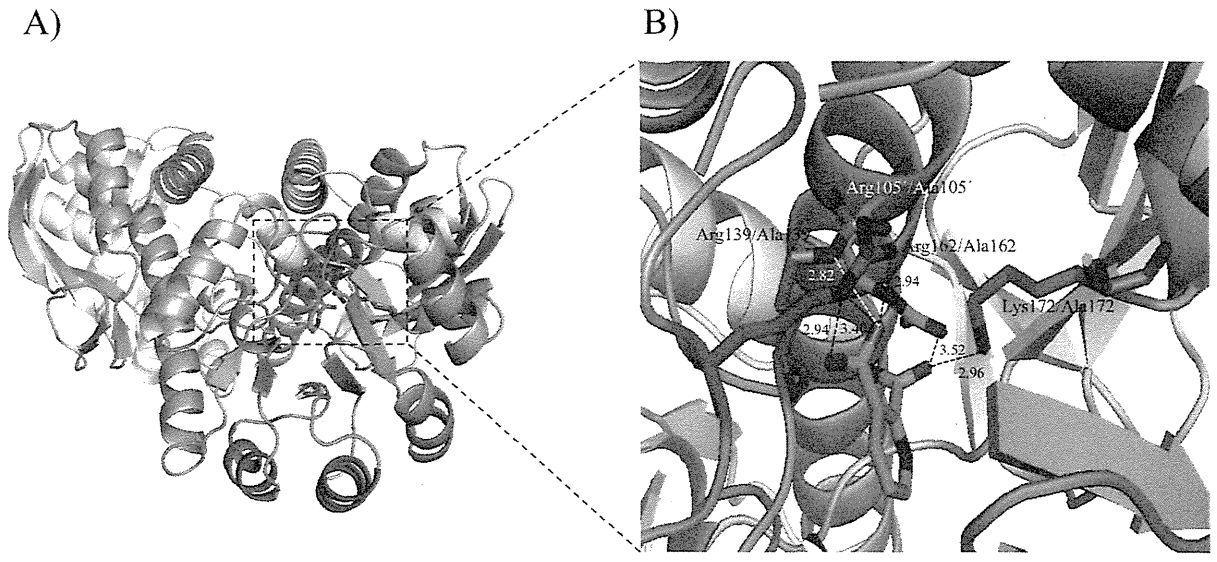

Figure 6. The QA binding mode in MtQAPRTase. The binding mode of QA is shown within the catalytic site of MtQAPRTase and the mutated amino acids (Arg105′Ala, Arg139Ala, Arg162Ala, Lys172Ala, and His175Ala) used in this study are shown. The A subunit of MtQAPRTase is depicted in light orange while the B subunit is depicted in pale cyan. The overall structures and the catalytic site on MtQAPRTase are shown on the left and right, respectively. The dotted line indicates hydrogen bonding, and the distance between amino acid residues and QA is indicated as well.
doi:10.1371/journal.pone.0100062.g006

A)

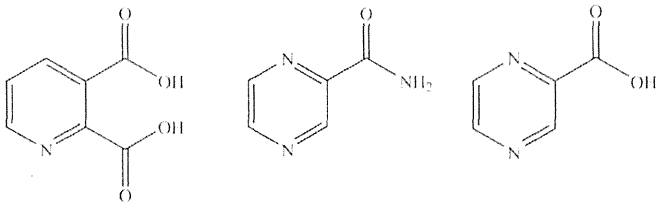

Quinolinic acid (QA) Pyrazinamide (PZA) Pyrazinoic acid (POA)

B)

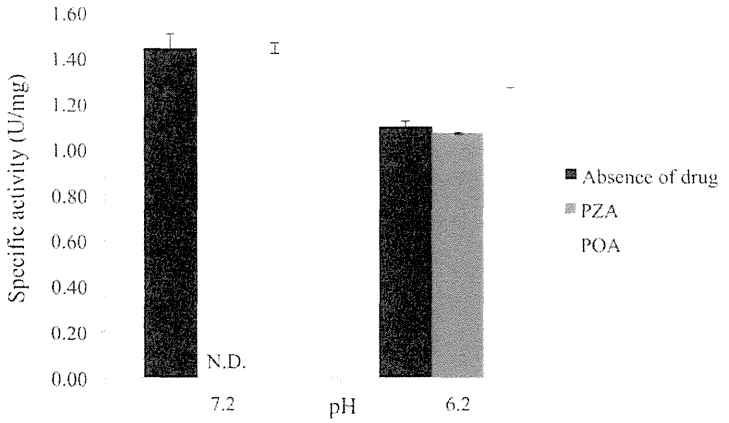

C)

	$IC_{50}s^{a}$ (mM)	
	pH 7.2	pH 6.2
PZA	0.38±0.02[b]	1.37±0.01
POA	3.45±0.05	> 20

[a] The values for the drug concentrations required to inhibit the MtQAPRTase activities by 50%.

[b] as ± means standard errors of three independent determinations.

Figure 7. Inhibitory effect of PZA or POA on MtQAPRTase activity and the calculated IC_{50} values. (A) Chemical structures of QA, PZA, and POA are shown. Either 1 mM of PZA or POA was incubated with MtQAPRTase at pH 7.2 (B, left) and pH 6.2 (B, right) at 37°C for 30 min. After incubation, reactions were stopped and the products analyzed using HPLC. The IC_{50} values are indicated in (C). N.D. mean not detected. Data from three separate experiments are represented as mean ± standard error.
doi:10.1371/journal.pone.0100062.g007

residues play important roles in QA binding and catalysis of QAPRTase activity.

Inhibitory effects of MtQAPRTase activity by PZA/POA and IC_{50} values

Because PZA and POA are structural analogs of QA (Fig. 7A), we predicted that these molecules may be substrates or inhibitors of MtQAPRTase. When PZA or POA were added to reaction mixtures instead of QA or PRPP, no new peaks were detected (data not shown), indicating that they are not substrates. To determine the inhibitory effects of PZA and POA on MtQAPRTase activity, PZA or POA was incubated with MtQAPRTase under different pH conditions (pH 7.2 and 6.2). Initially, we investigated the concentrations of PZA and POA under neutral (pH 7.2) and weak acidic (pH 6.2) conditions. PZA and POA were tested for their abilities to inhibit MtQAPRTase between the concentrations of 0.1 and 3.0 mM (data not shown). Figure 7B shows the results of a representative inhibitory QAPRTase assay containing 1 mM of PZA or POA at pH 7.2 (Fig. 7B left) and pH 6.2 (Fig. 7B right), respectively. Interestingly, the inhibitory effect of PZA at pH 7.2 condition was dramatically higher than at pH 6.2 condition and that of POA at any pH value. IC_{50} values of PZA and POA are summarized in Fig. 7C. The IC_{50} values of PZA were 0.38±0.02 and 1.37±0.01 mM at pH 7.2 and 6.2, and those of POA were 3.45±0.05 and >20 mM at pH 7.2 and 6.2, respectively. Using the IC_{50} values, the K_i values were estimated by a web-based tool [41], (http://botdb.abcc.ncifcrf.gov/toxin/kiConverter.jsp). The K_i values of PZA were 19.2 μM and 69.4 μM at pH 7.2 and 6.2, respectively, and that of POA was 174.7 μM at pH 7.2.